

Geophone orientation analysis in a 3D VSP survey, Alberta

Peter Gagliardi and Don C. Lawton

ABSTRACT

Geophone orientation azimuths were found from 3D and 2D VSP data, acquired near Lousana, Alberta, in order to examine any dependence of computed geophone orientation on source-well offset or azimuth. Additionally, a comparison was made between analytic and hodogram methods. The 2D dataset consisted of three lines; the standard deviation for this survey was 0.67° for all lines, 0.45° for the east line, 0.41° for the southeast line and 0.55° for the south line. Removal of sources less than 500 m (approximately 1/2 of the geophone depth) significantly improved the scatter in this dataset. Standard deviation in orientation azimuths for all lines was found to be 0.90° using the hodogram method; thus, while the both methods performed well, the analytic method produced more consistent results. The 3D dataset was divided based on source-well azimuth into bins with centers trending 0° - 180° , 45° - 225° , 90° - 270° and 135° - 315° . There appeared to be little dependence on source-well sector azimuth, which is expected for flat, isotropic geology near the well. Standard deviation in orientation azimuths were found to be 1.74° using the full 3D dataset. Offsets were binned into ranges of 0-600 m, 600-950 m, 950-1300 m, 1300-1650 m and greater than 1650 m. Scatter in rotation angles was shown to be strongly dependent on offset, with the most constrained results in the 1300-1650 m offset bin. The optimal offset range for geophone orientation calibration was found to be between 1 and 2 times the receiver depth.

INTRODUCTION

Multi-component borehole geophones are used traditionally in the acquisition of vertical seismic profiles (VSP) and increasingly in microseismic monitoring, in which data recorded by these geophones are used to determine the hypocentres of microseismic events associated with hydraulic fracturing. However, when deploying these geophones into a well they will rotate, resulting in an unknown orientation of their horizontal components once installed. In order to determine the orientation of these borehole geophones, calibration surveys are required, often using surface seismic sources. The fidelity of these calibrations will affect the accuracy in locating microseismic events (Eisner et al., 2009) as well as for VSP imaging and analysis, particularly for PS waves (Müller and Soroka, 2010). Geophone orientation analysis also has applications to ocean bottom seismic experiments; Li and Yuan (1999) performed such an analysis on seismic data acquired with 3-C ocean bottom nodes in the North Sea. In this project, we determined the orientation azimuths of 3-component receivers in a downhole tool from first arrival analysis of the horizontal components. Results were examined for consistency, for a large range of surface source offsets and azimuths. The methods that were used to find geophone orientation were an analytic method developed by DiSiena et al. (1984), as well as hodogram analysis, both windowed on the direct P-wave arrivals.

Finally, note that this study is an extension of a previous study by Gagliardi and Lawton (2011).

SURVEY GEOMETRY

In July 2007, several vertical seismic profile (VSP) surveys were acquired for EnCana Corporation, using a vertical well near Lousana, Alberta; these surveys were comprised of a zero offset VSP, three 2D walkaway VSP's and a 3D VSP. The walkaway survey consisted of three lines, trending south, southeast and east; each line had 10 source locations with a maximum source-well offset of 1391 m (FIG. 1). The 3D survey consisted of 249 source locations with a maximum offset of 3255 m (FIG. 2). Both surveys used two coupled geophone tools, each with eight 3-component geophones, and 2 kg of dynamite at a depth of 15 m was used as a source. All source locations in the walkaway dataset were repeated 4 times using different tool levels, resulting in a total of 64 receiver locations. The 3D VSP was performed separately after the walkaway, using a single tool position. The receiver depth range for the walkaway survey was 468 m to 1420 m, and the depth range of the 3D survey was 717 m to 944 m.

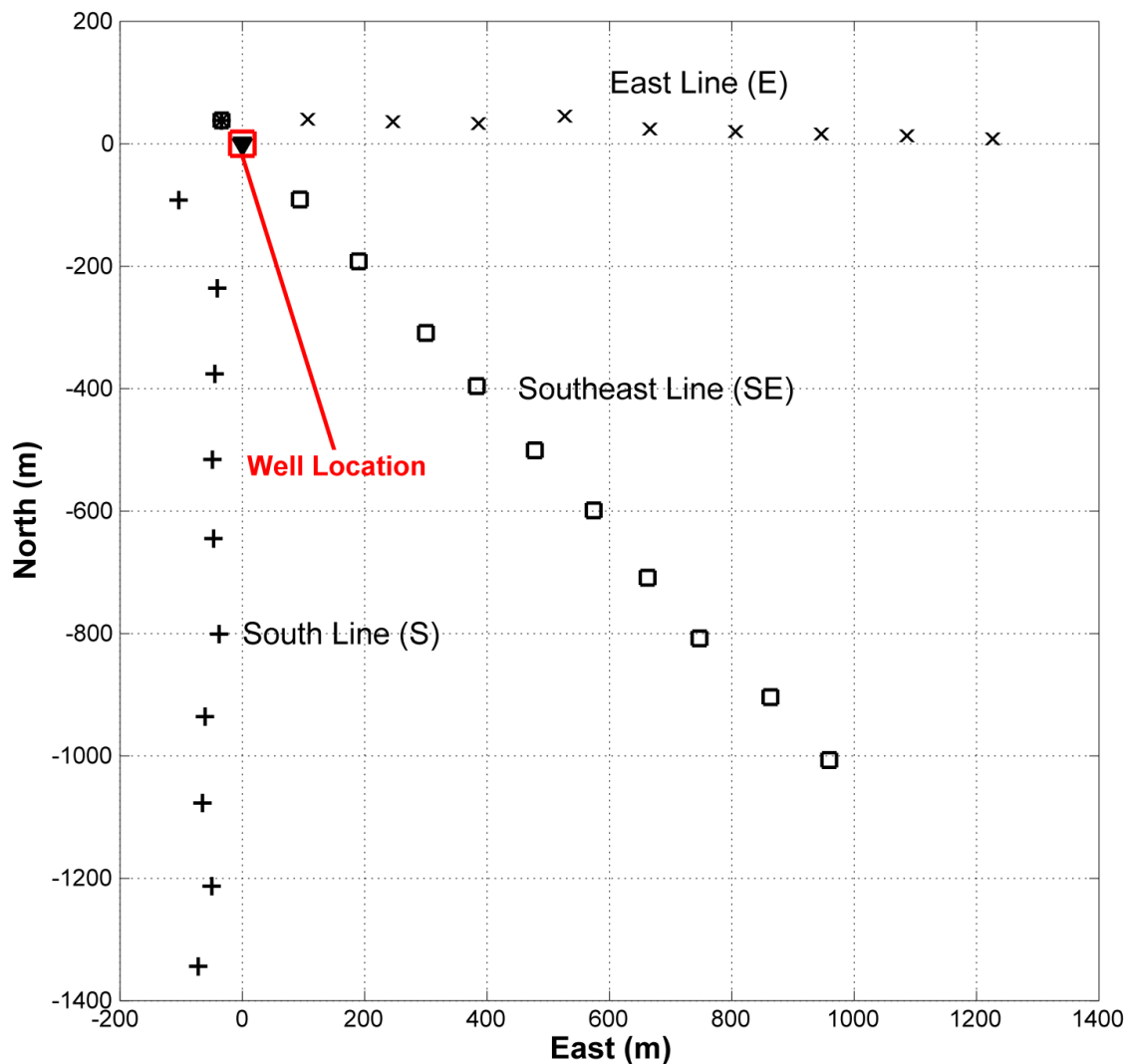


FIG. 1. Surface geometry for the 2D walkaway VSP surveys. Coordinate origin is at the well. Lines are identified as E, SE and S.

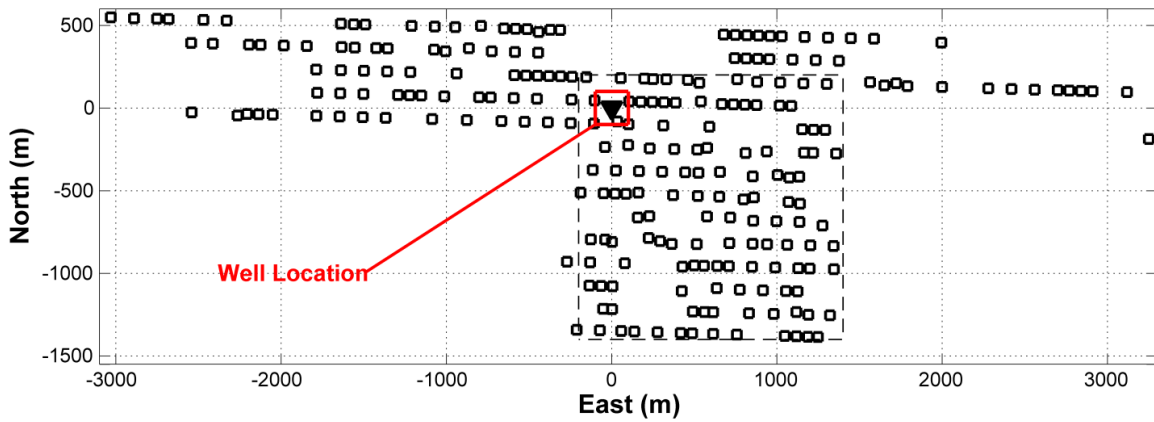


FIG. 2. Surface geometry for the 3D VSP survey, showing an outline of the 2D walkaway VSP area. Coordinate origin is at the well.

An example of a common shot gather from a near-offset shot from the east-trending line is shown in FIG. 3; an example of a common shot gather from the 3D VSP survey, again from a near-offset shot, is shown in FIG. 4. It should be noted that data from the receiver at position 2 of each level were not used in the analysis, as there was a problem with one of its horizontal components. The VSP surveys were undertaken primarily for imaging deep coal seams, but in this study we focus on a statistical analysis of the geophone orientations in the well.

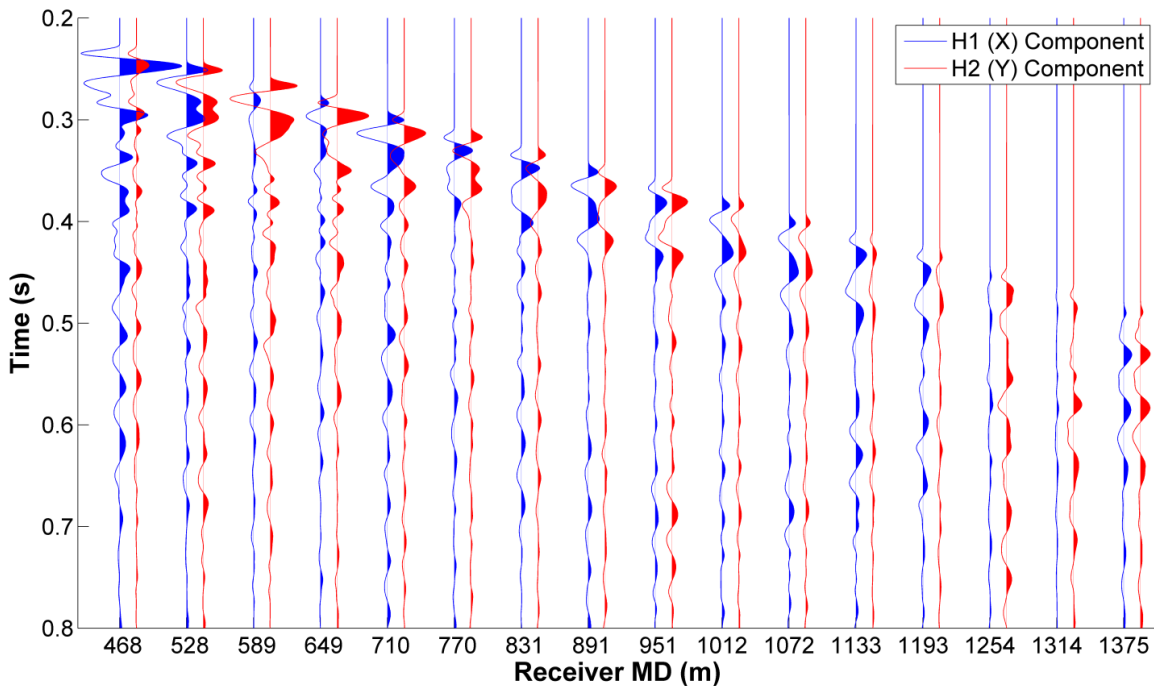


FIG. 3. Raw shot gather from a near offset shot of the East line of the 2D walkaway VSP survey; coordinates are 33 m north and 386 m east of the well. H1-component is shown in blue and H2-component is shown in red. No gain has been applied.

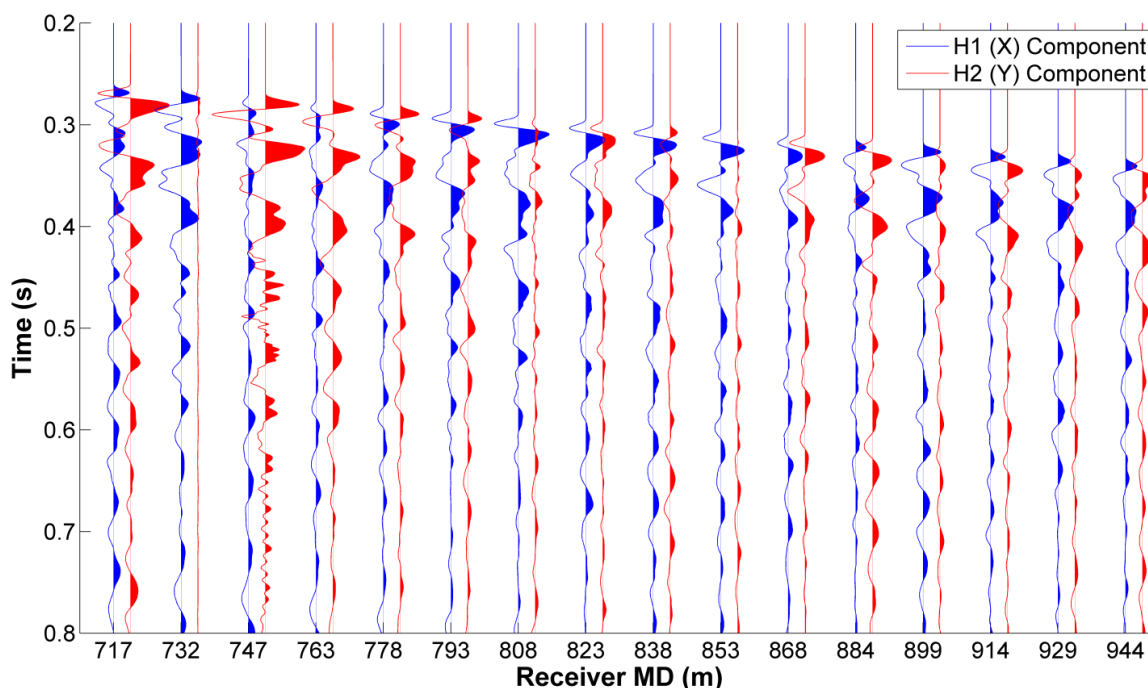


FIG. 4. Raw shot gather from a near offset shot of the 3D VSP survey; coordinates are 81 m south and 33 m east of the well. H1-component is shown in blue and H2-component is shown in red. No gain has been applied.

ROTATION METHODS

An analytic solution for calculation of geophone rotation angle is given by (DiSiena et al., 1984):

$$\tan 2\theta = \frac{2H_1 \otimes H_2}{H_1 \otimes H_1 + H_2 \otimes H_2}, \quad (1)$$

where \otimes is a zero-lag crosscorrelation operator, H_1 and H_2 are the windowed horizontal component data and θ is the angle between the H1-component and source. For this study, a window of 100 ms was used, beginning at the onset of first arrival energy of the downgoing wavefield. In the case of a vertical well, this angle can be converted into an azimuth relative to geographic north, ϕ_r , by

$$\phi_r = \phi_s + \theta, \quad (2)$$

where ϕ_s is the source azimuth from the well.

In addition to the analytic solution, geophone orientation analysis was also undertaken using hodograms, using the same analysis window as that used in the method described above. FIG. 5 shows sample hodograms for a near and far offset shot from the 2D walkaway dataset, along with the lines of best fit. The source-receiver angle is found by taking the inverse tangent of the slope.

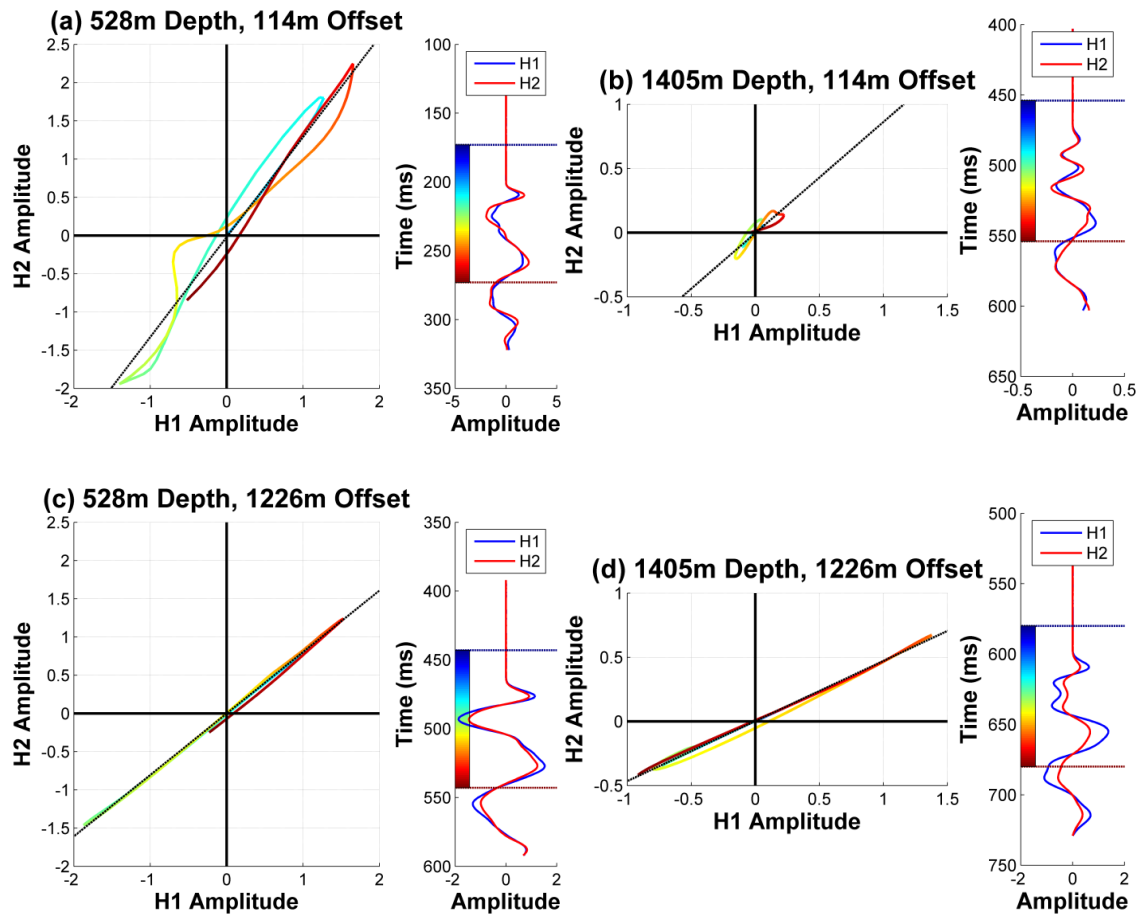


FIG. 5. Examples of hodograms from the East line of the 2D walkaway VSP data.

2D WALKAWAY RESULTS

FIG. 6 shows the results of geophone orientation azimuths calculated using the analytic method, for a subset of receivers. Each of the three walkaway datasets is shown in a different color; there were an equal number of data points for all three lines, and they each had a similar offset distribution. FIG. 6 shows that the orientation azimuths have no clear dependence on the orientation of the line chosen, and agreement is quite good between each of the lines. More scatter can be seen in the nearer source offsets, and the deeper receiver positions retain this scatter for larger source-well offsets. These effects are related to the incoming angle of the direct P-wave energy at the receiver: small receiver depths and large source-well offsets result in incident angles at the receiver close to 90° , resulting in horizontal components recording a greater proportion of the direct energy, thereby reducing scatter in analysis of geophone orientation azimuth.

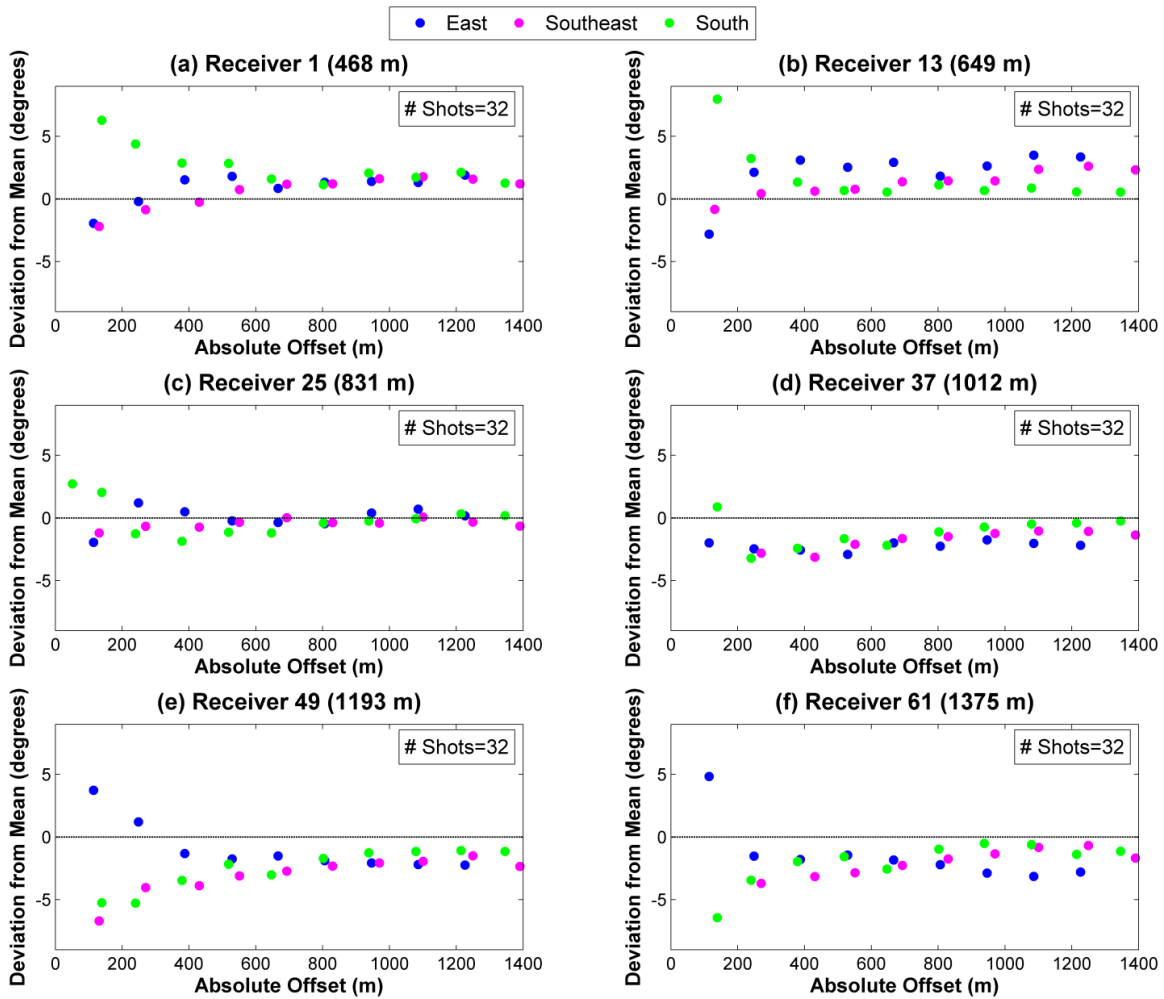


FIG. 6. Variation in geophone orientation azimuths for several receiver positions, calculated using the analytic method, for the 2D walkaway dataset colored by line; E is shown in blue, SE is shown in magenta and S is shown in green.

Table 1 summarizes the statistical analysis of a subset of receivers in the 2D walkaway dataset, using 3σ , 2σ and 1σ cutoff values for outlier removal, as well as removal of data points from source-well offsets smaller than 500 m. There is a significant decrease in scatter of orientation azimuth when reducing the outlier cutoff from 3σ to 2σ , whereas reducing the cutoff from 2σ to 1σ only slightly decreases scatter. Removal of data points from near offsets shows the least scatter, quantitatively confirming the trend noticed in FIG. 6. Table 2 provides a comparison of orientation statistics of far offset data using the analytic and hodogram methods for the same subset of receivers. Direct comparison of standard deviation values is shown in FIG. 7a, and the differences between means calculated using the two methods are shown in FIG. 7b. Mean values calculated using the two methods are generally within $\pm 0.5^\circ$ of each other, and scatter is slightly better when using the analytic method. Finally, FIG. 8 shows the standard deviation for each receiver, calculated using both methods. Overall, the two methods produced similar results; thus, results using the hodogram method will be omitted for the 3D VSP.

Table 1. Geophone orientation statistics for a subset of the 2D dataset made using the analytic method, for different outlier conditions. Means and standard deviations are in degrees.

Receiver Number	Depth (m)	3σ		2σ		1σ		Far Offsets	
		Mean	S. Dev	Mean	S. Dev	Mean	S. Dev	Mean	S. Dev
1	468	275.1	4.65	276.5	1.63	276.3	1.35	276.6	0.48
13	649	195.8	5.64	197.5	1.82	197.3	1.38	197.5	1.00
25	831	229.1	1.20	228.8	0.84	228.8	0.51	228.9	0.47
37	1012	119.5	6.41	117.6	1.71	117.8	0.95	118.0	0.71
49	1193	242.7	7.23	240.5	1.91	240.5	1.91	240.8	0.59
61	1375	317.1	6.93	315.0	2.21	315.3	1.79	315.4	0.82
Average			5.22		1.63		1.26		0.67

Table 2. Comparison of geophone orientation statistics for a subset of the 2D dataset for different analysis methods. Means and standard deviations are in degrees.

Receiver Number	Depth (m)	Analytic		Hodogram		Difference	
		Mean	Std. Dev	Mean	Std. Dev	Mean	Std. Dev
1	468	276.6	0.48	277.3	1.27	-0.69	-0.79
13	649	197.5	1.00	197.5	1.06	0.01	-0.06
25	831	228.9	0.47	229.1	0.51	-0.17	-0.04
37	1012	118.0	0.71	118.1	0.72	-0.02	-0.01
49	1193	240.8	0.59	240.8	0.58	-0.04	0.01
61	1375	315.4	0.82	315.4	0.86	0.01	-0.03
Average			0.67		0.90		-0.23

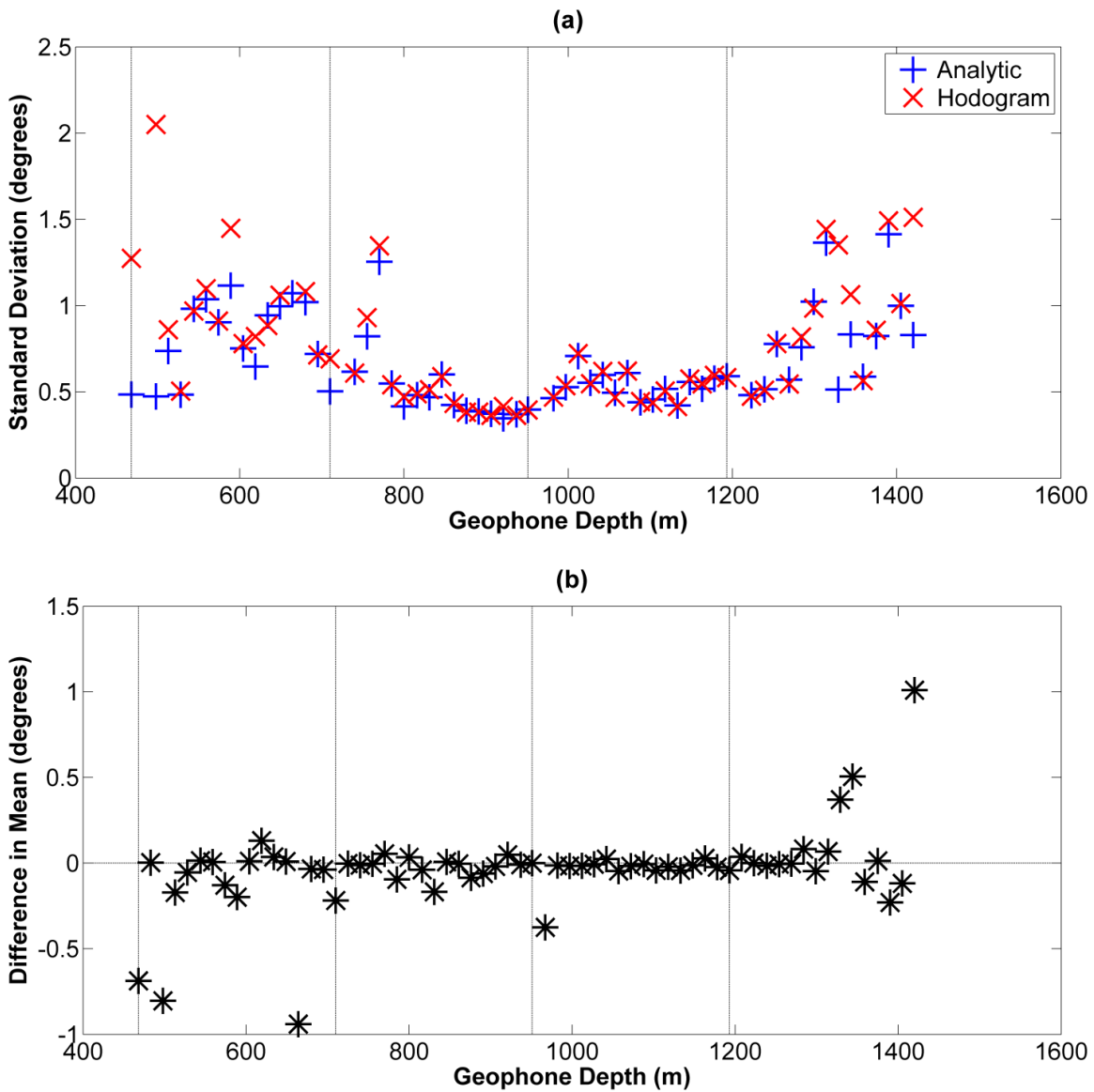


FIG. 7. (a) Standard deviations for each receiver using the analytic (blue) and hodogram (red) methods. (b) Differences in mean orientation for each receiver; value is calculated by subtracting the hodogram mean from the analytic mean. Vertical lines are represent the top of each tool level.

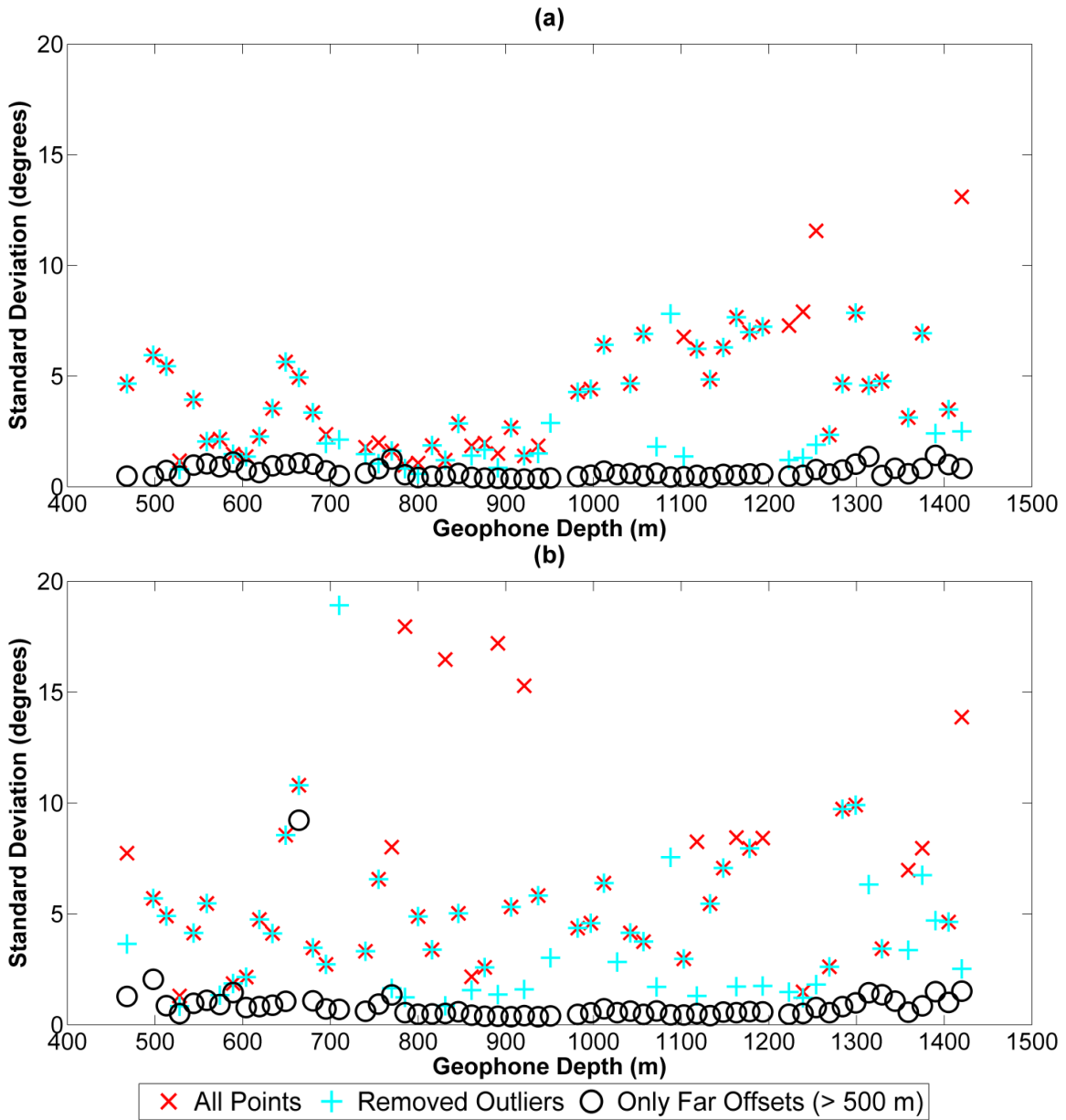


FIG. 8. Orientation standard deviations for each receiver calculated using the (a) analytic and (b) hodogram methods. Red is calculated using all data points, cyan after removal of outliers and black after removal of outliers and near offsets less than 500 m.

3D WALKAWAY RESULTS

Sector analysis

In order to examine consistency of the relationship of geophone orientation and source-well azimuth, the 3D dataset was divided into 4 sectors based on the source-well azimuth (FIG. 9). Sector centers were lines trending at 0° - 180° (Sector 1), 45° - 225° (Sector 2), 90° - 270° (Sector 3) and 135° - 315° (Sector 4) azimuths. As shown in FIG. 9, due to the acquisition geometry, there was a large variation in the number of source locations between each sector. FIG. 10 shows orientation azimuths calculated using the analytic method, plotted against offset. For all receivers, the calculated azimuths become much less scattered beyond about 500 m source-well offset, or about 1/2 of the geophone depth. It is not possible to discern any noticeable difference between angles calculated in each of the sectors; however, the lower number of source locations and more restricted offsets in Sectors 1, 2 and 4 is noticeable.

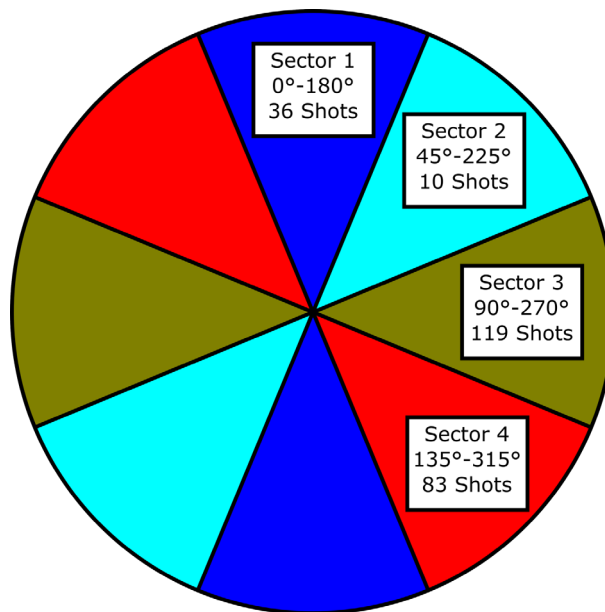


FIG. 9. Azimuthal sectoring for the 3D walkaway VSP survey.

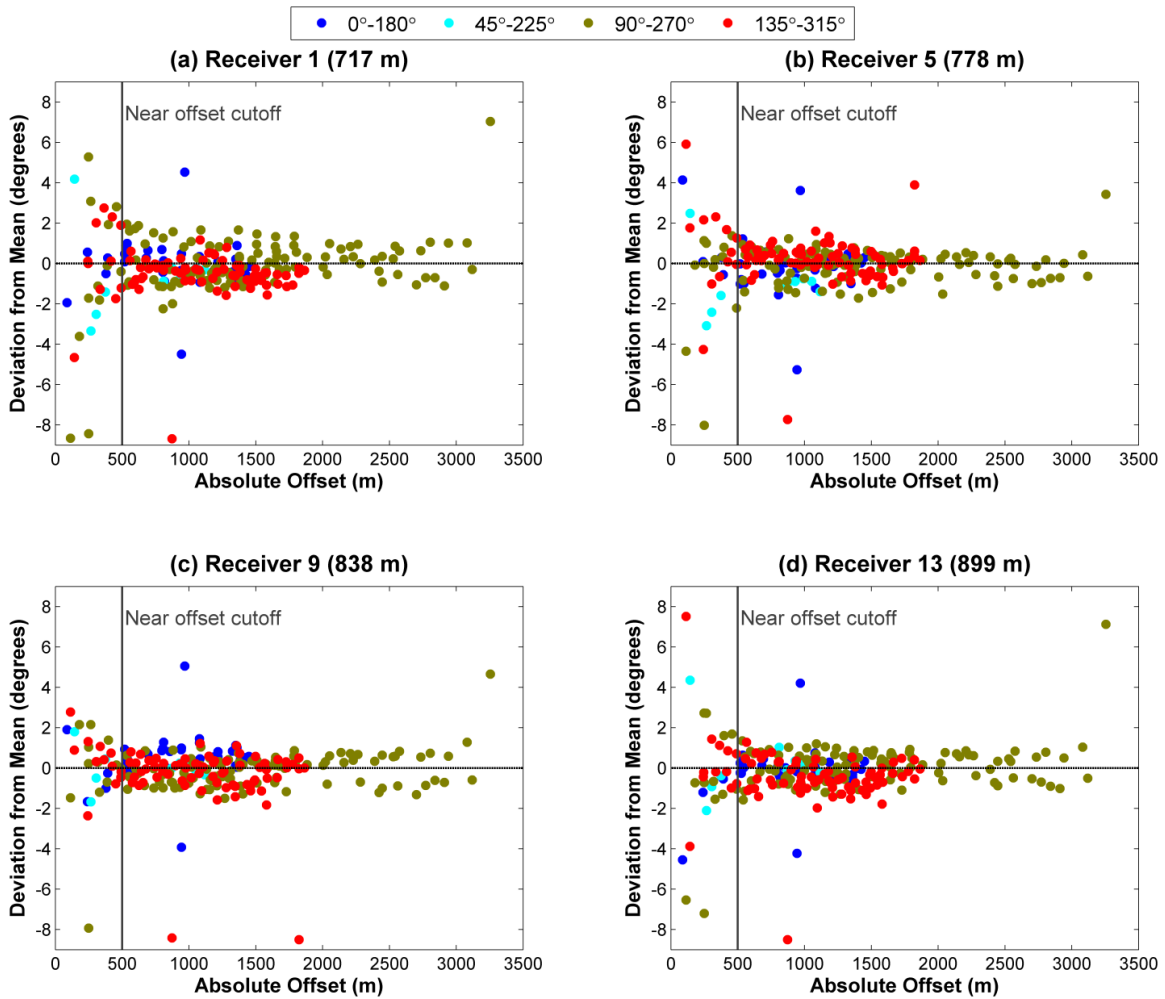


FIG. 10. Deviation in geophone orientation azimuths, versus source-well offset, for several receivers in the 3D dataset calculated using analytic method, colored by bin; 0° - 180° is shown in blue, 45° - 225° is shown in cyan, 90° - 270° is shown in yellow and 135° - 315° is shown in red.

FIG. 11 shows orientation azimuths plotted against source-well azimuth. When viewed this way, there appears to be a subtle increase of calculated orientation angle at larger source-well azimuths. Histograms of orientation azimuth are shown in FIG. 12 (all offsets) and FIG. 13 (offsets greater than 500 m). Finally, FIG. 14 shows a radial plot of results for a subset of the geophones; data points are plotted in plan view, showing the calculated azimuth as a function of source-well offset. This display provides a clear picture of the relationship between offset, orientation angle error and overall deviation for of each shot.

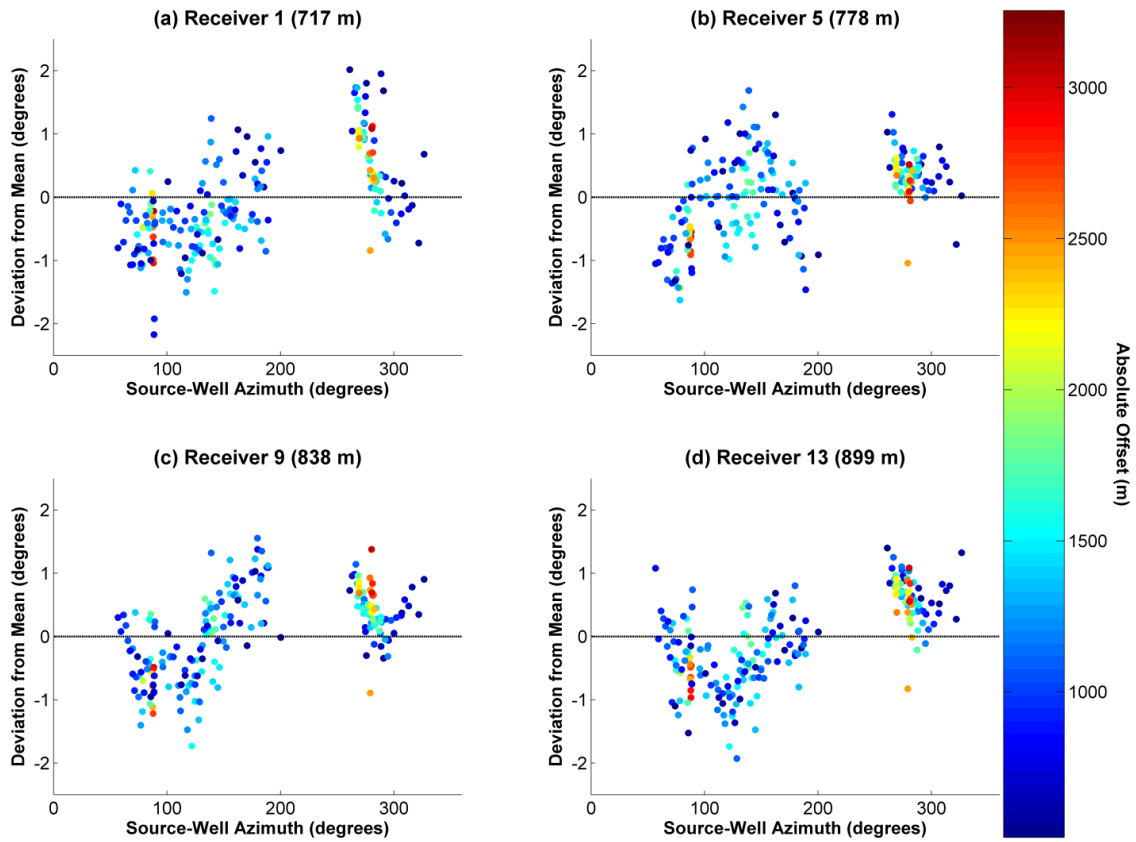


FIG. 11. Deviation in geophone orientation azimuths, versus source-well azimuth, for several receivers in the 3D dataset calculated using analytic method, for 3D walkaway colored by offset. Hotter colors represent far offsets, cooler colors represent near offsets.

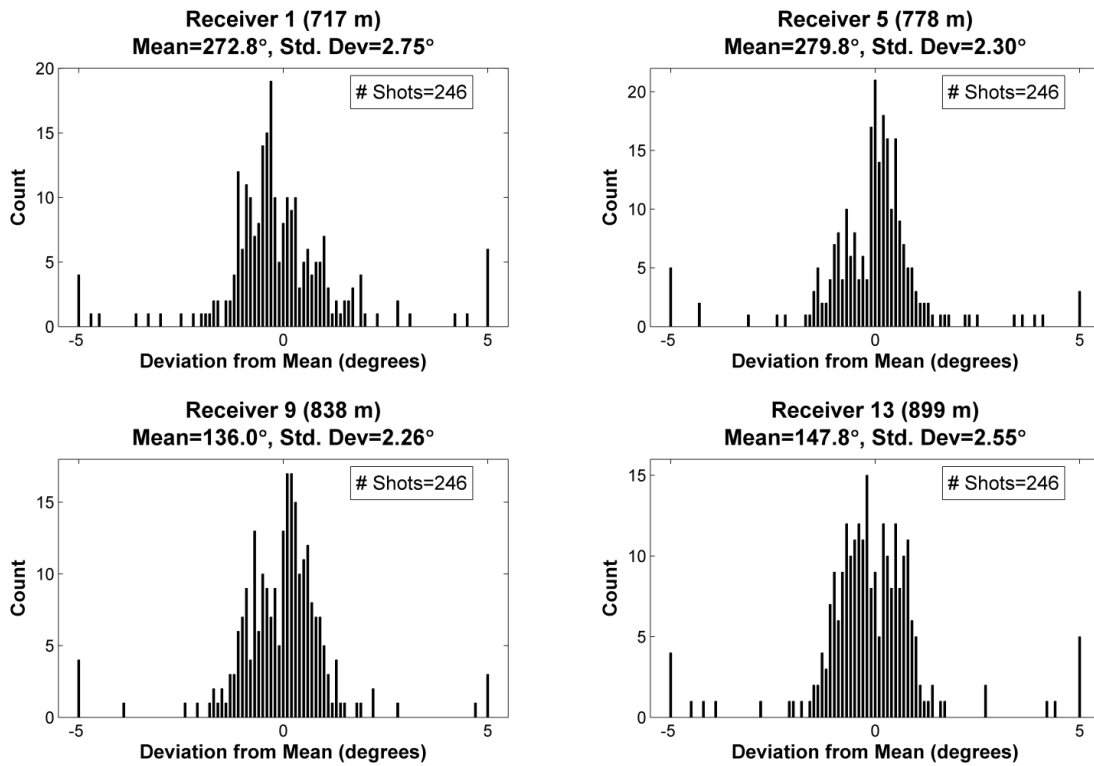


FIG. 12. Histograms of orientation azimuth for several receivers in the 3D dataset calculated using analytic method.

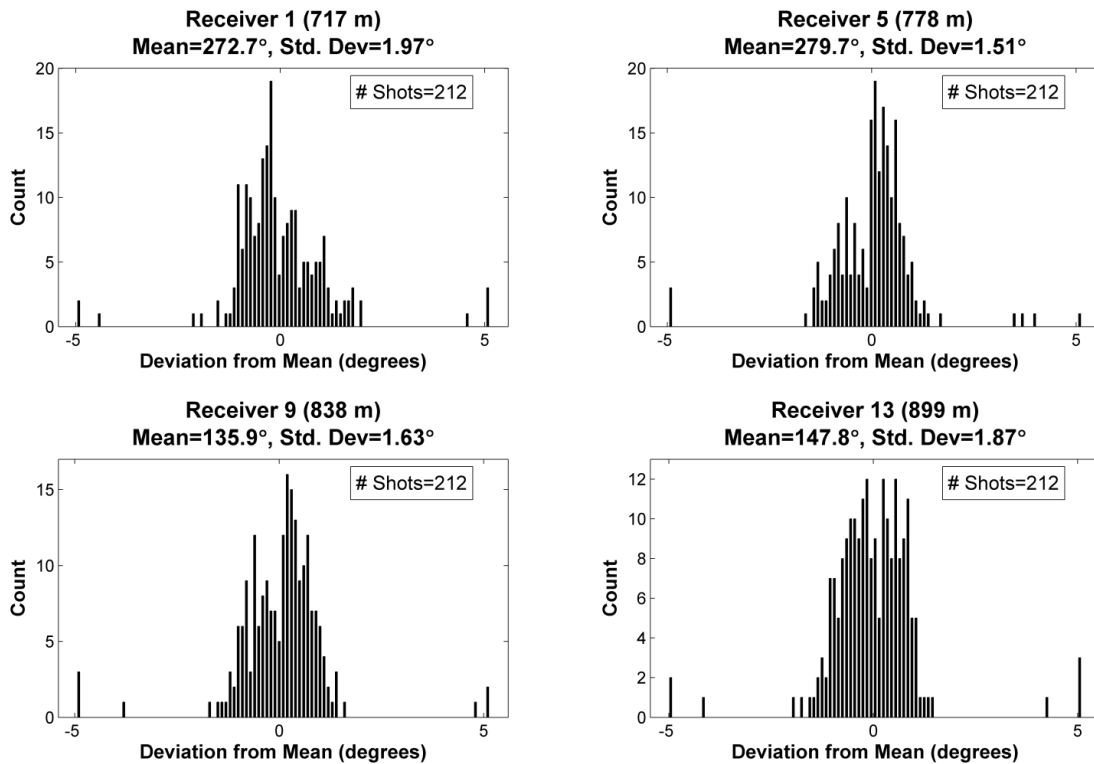


FIG. 13. Histograms of orientation azimuth for several receivers in the 3D dataset calculated using analytic method, after rejection of near offset shots (less than 500 m).

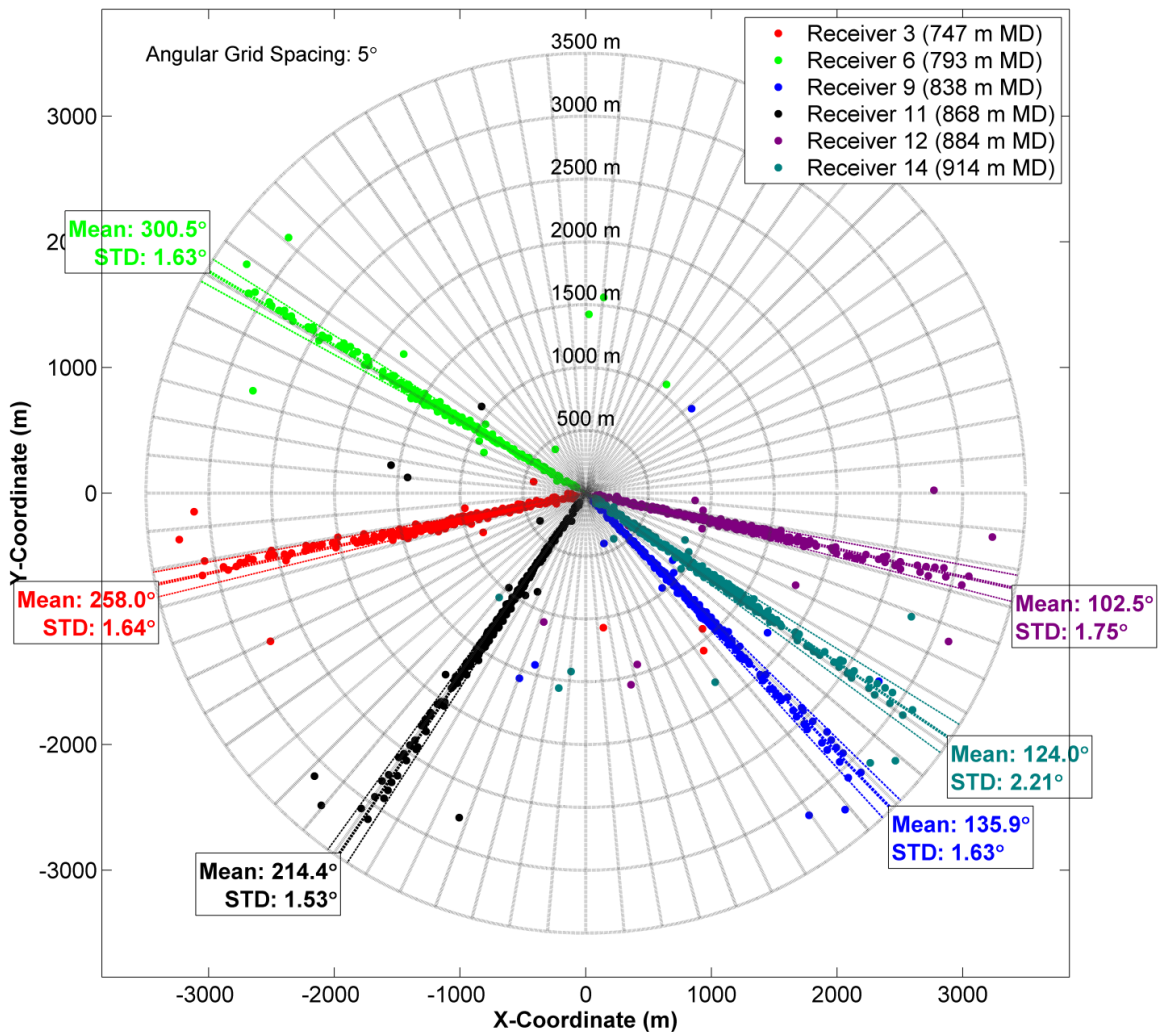


FIG. 14. Radial plot of geophone orientation azimuths for a subset of receivers. All shots are shown, but statistics are found from far offset data only. Envelope lines represent one standard deviation. Radial spacing is 500m, angular spacing is 5°.

Geophone orientation statistics

Table 3 shows orientation azimuth means and standard deviations, for the complete 3D dataset, using the analytic method. Table 4 shows the binned orientation azimuth means and standard deviations, after the removal of outliers and source-well offsets less than 500 m from the well. The removal of outliers was done separately for the binned and unbinned calculations; this is apparent through the different standard deviations. Examining the mean orientation angle for each receiver across bins, slight differences can be seen, but none of the differences is greater than 2° and there does not appear to be any consistent trend in the differences. The maximum mean angle difference is less than 1° for most receivers, despite the large variety in bin sizes. FIG. 15 shows the standard deviation for each bin, using the analytic method, as a function of receiver depth.

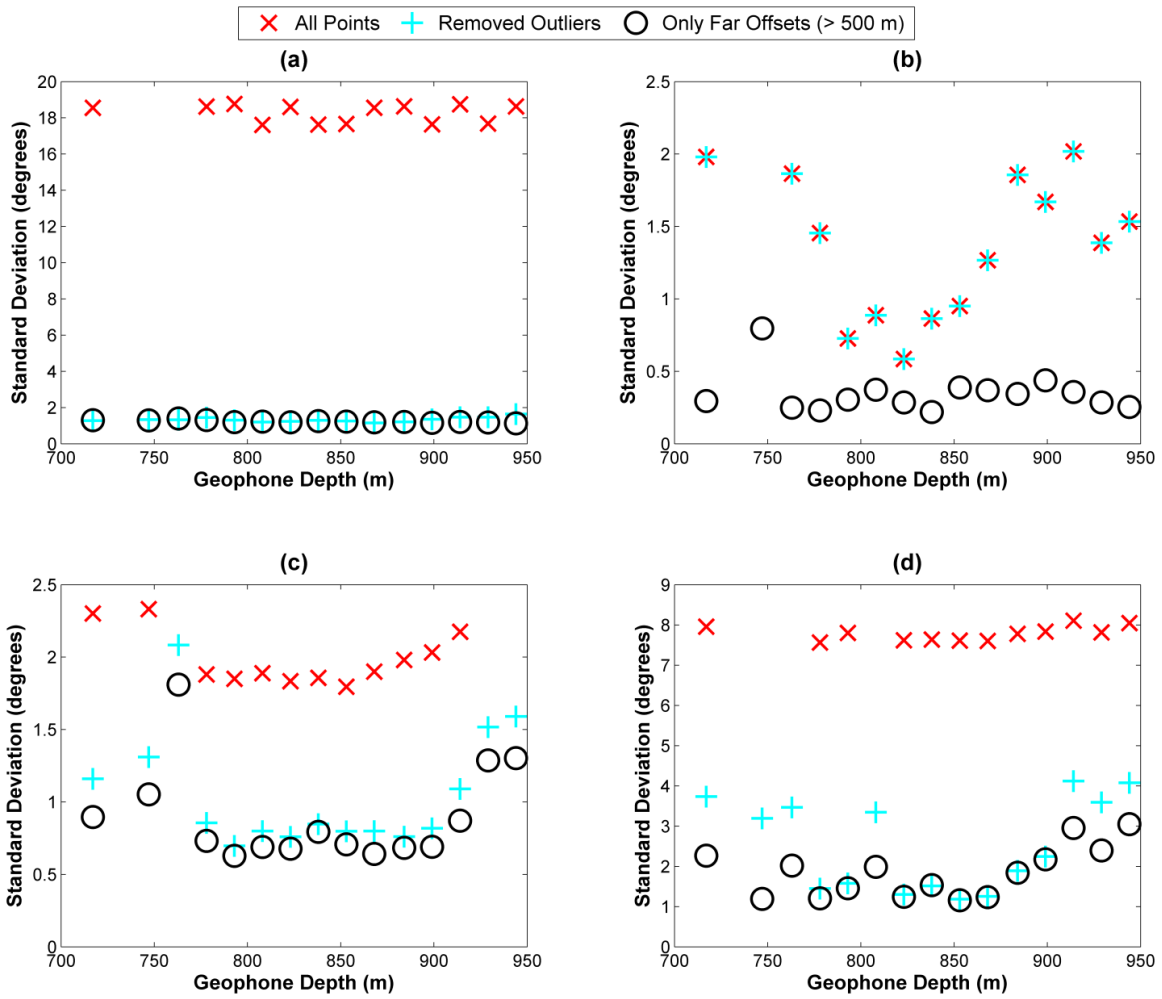


FIG. 15. Orientation azimuth standard deviations for each receiver calculated using the analytic method, using azimuthal sectoring. Red is calculated using all data points, cyan after removal of outliers and black after removal of outliers and near offsets less than 500 m.

Table 3. Geophone orientation statistics for 3D dataset made using the analytic method. Means and standard deviations are in degrees.

Receiver Number	Depth (m)	All		Removed Outliers		Far	
		Mean	Std. Dev	Mean	Std. Dev	Mean	Std. Dev
1	717	273.6	8.63	272.8	2.75	272.7	1.97
2	732	56.0	56.93	56.0	56.93	55.8	57.51
3	747	256.8	12.04	258.1	2.62	258.0	1.64
4	763	261.5	13.33	263.1	2.60	263.1	1.82
5	778	280.7	8.49	279.8	2.30	279.7	1.51
6	793	301.5	8.56	300.6	2.32	300.5	1.63
7	808	163.1	10.15	163.7	2.40	163.6	1.79
8	823	195.5	8.49	194.6	2.19	194.5	1.50
9	838	136.2	8.06	136.0	2.26	135.9	1.63
10	853	158.6	8.07	158.3	1.52	158.3	1.47
11	868	215.3	8.48	214.4	2.23	214.4	1.53
12	884	103.5	8.56	102.6	2.43	102.5	1.75
13	899	148.0	8.16	147.8	2.55	147.8	1.87
14	914	124.9	8.70	124.0	2.89	124.0	2.21
15	929	136.1	9.81	135.5	2.41	135.4	1.71
16	944	118.7	10.58	117.4	2.69	117.3	2.02
Average			9.34		2.41		1.74

Table 4. Geophone orientation statistics for binned 3D dataset made using the analytic method. Means and standard deviations are in degrees.

Receiver Number	Depth (m)	0-180		45-225		90-270		135-315	
		Mean	S. Dev	Mean	S. Dev	Mean	S. Dev	Mean	S. Dev
1	717	272.8	1.30	272.3	0.30	272.8	0.90	272.4	2.26
2	732	-3.8	11.75	61.7	3.73	87.2	9.87	37.2	80.74
3	747	258.5	1.29	258.6	0.80	258.3	1.05	257.4	1.19
4	763	262.5	1.40	262.3	0.25	263.1	1.81	263.3	2.02
5	778	279.5	1.32	278.8	0.23	279.7	0.73	279.9	1.20
6	793	300.3	1.19	300.8	0.30	300.9	0.63	299.9	1.46
7	808	164.5	1.22	163.8	0.37	163.6	0.69	163.3	1.99
8	823	194.9	1.19	194.7	0.29	194.6	0.68	194.3	1.25
9	838	136.7	1.25	136.0	0.22	135.9	0.79	135.6	1.53
10	853	158.3	1.22	158.7	0.39	158.5	0.71	158.0	1.16
11	868	214.8	1.19	214.5	0.37	214.5	0.64	214.1	1.23
12	884	102.6	1.21	102.8	0.34	102.8	0.68	102.1	1.84
13	899	147.8	1.16	148.0	0.44	147.9	0.69	147.5	2.18
14	914	124.0	1.20	123.9	0.36	124.1	0.87	123.7	2.96
15	929	135.7	1.17	135.5	0.29	135.5	1.29	135.3	2.40
16	944	117.6	1.13	117.5	0.25	117.4	1.30	117.1	3.05
Average			1.23		0.35		0.90		1.85

Offset analysis

In order to more closely examine the relationship between offset and scatter in orientation angle, data were binned at different offset panels: 0-600 m, 600-950 m, 950-1300 m, 1300-1650 m and greater than 1650 m. Bins were chosen to have a consistent number of shots, encompassing 45, 47, 56, 46 and 47 source locations respectively. FIG. 16 shows the standard deviation as a function of offset bin and geophone depth. Though there is no consistent relationship between standard deviation and geophone depth, there is a strong relationship between the standard deviation and offset bin. Each receiver reaches a minimum scatter in the 1300-1650 m offset range; reasons for this are discussed later in this section. This is more closely examined in FIG. 17, which shows curves representing the 600-950 m, 950-1300 m and 1300-1650 m bins, and FIG. 18, which shows the overall standard deviation of all receivers for each bin. It is interesting to note that the two latter bins have markedly less scatter in orientation angle than results involving all offsets.

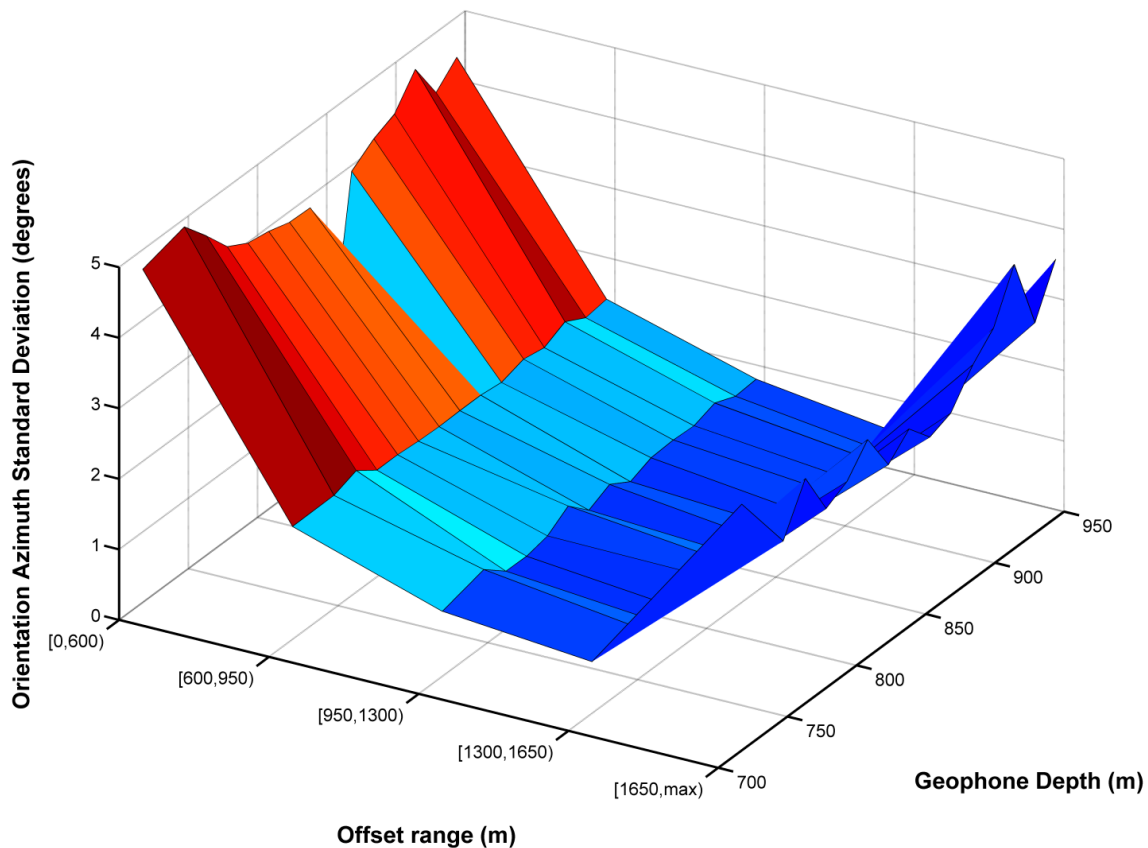


FIG. 16. Standard deviation of geophone orientation azimuth versus geophone depth and sectored offset range.

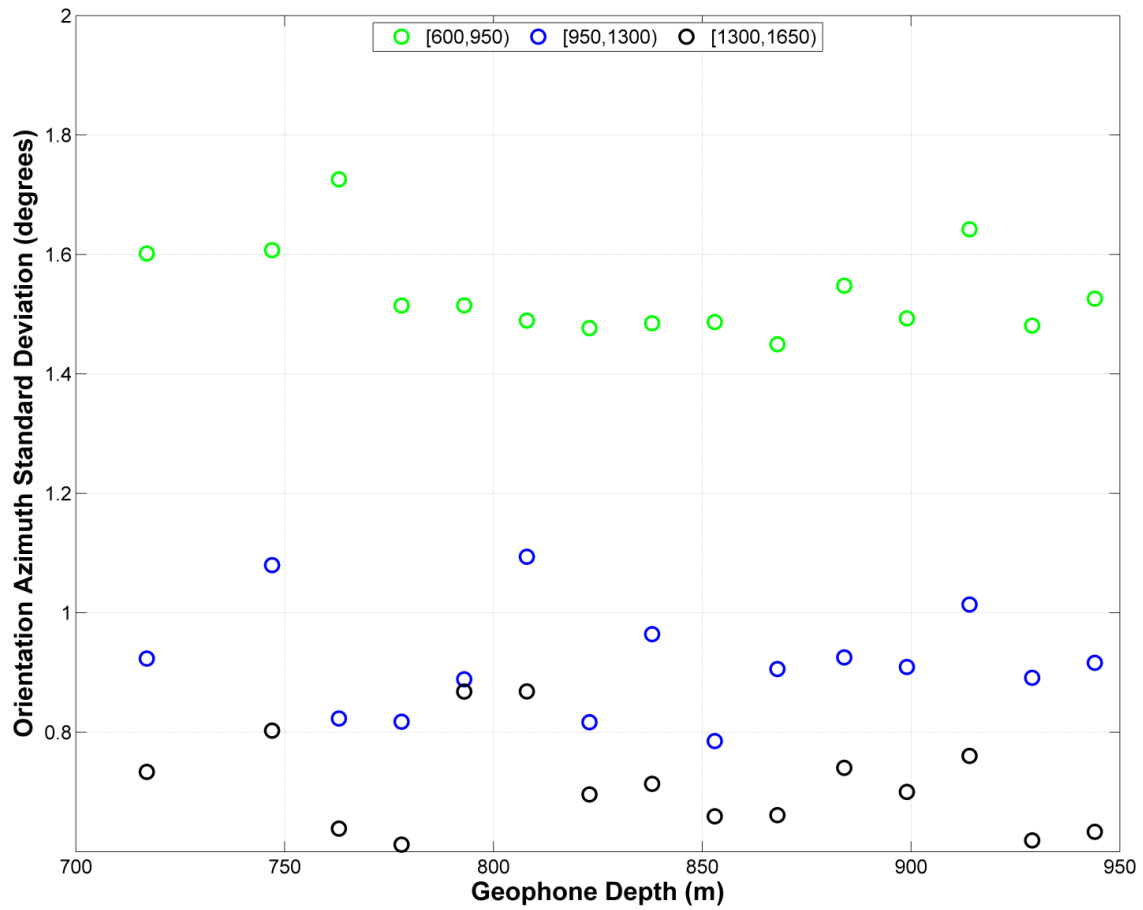


FIG. 17. Constant offset slices from FIG. 16, showing 600-950 m bin in green, 950-1300 m bin in blue, and 1300-1650 m bin in black.

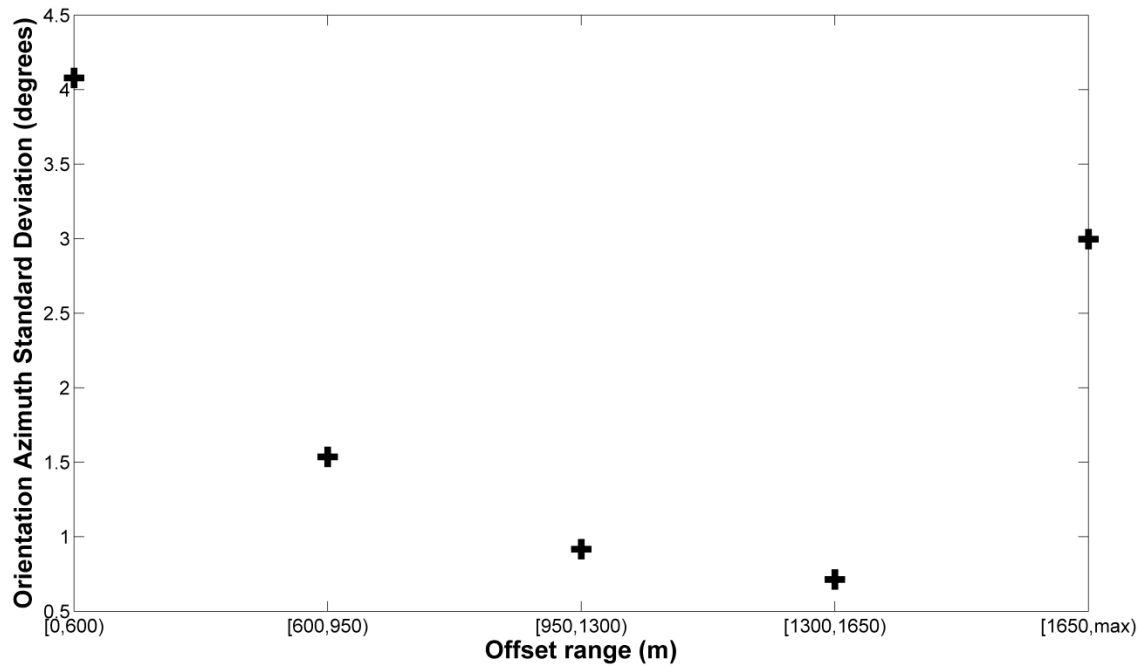


FIG. 18. Average standard deviation for all receivers (except receiver 2) at each offset bin.

Finally, in order to better understand the effects of source-well offset on the analysis of geophone orientation azimuth, a simple analytic model was devised. For a vertical well in a homogeneous, isotropic medium with a very high quality factor (FIG. 19), the amplitude of the direct P-wave arrival measured by the horizontal components will depend on two factors. Geometric spreading must be taken into account, which is given simply by:

$$\frac{A}{A_0} = \frac{1}{r} = \frac{1}{\sqrt{x^2+z^2}}, \quad (3)$$

where A is the amplitude at the receiver, and A_0 is the original amplitude. However, the amplitude measured by the horizontal components of the geophone will be a function of the angle θ , such that:

$$\frac{A_H}{A_0} = \frac{A}{A_0} \sin \theta = \frac{A}{A_0} \frac{x}{\sqrt{x^2+z^2}}, \quad (4)$$

where A_H is the horizontal amplitude at the receiver. Combining equations (3) and (4), the overall amplitude measured by the horizontal components of the geophones can be written as:

$$\frac{A_H}{A_0} = \frac{x}{x^2+z^2}. \quad (5)$$

Using equation (5), the relationship between the relative horizontal amplitude and the offset/depth ratio was examined (FIG. 20). The peak amplitude is predicted to occur at an offset/depth ratio of 1, supporting the results of the 3D walkaway; offset/depth ratios with amplitudes of at least -2 dB from the peak occur between 0.5 and 2, again supporting results of the 3D walkaway.

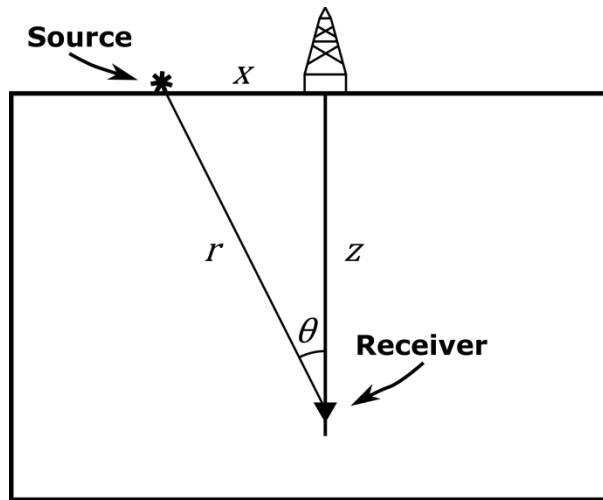


FIG. 19. Diagram illustrating geometry of a surface source and a borehole geophone embedded in a homogeneous, isotropic medium.

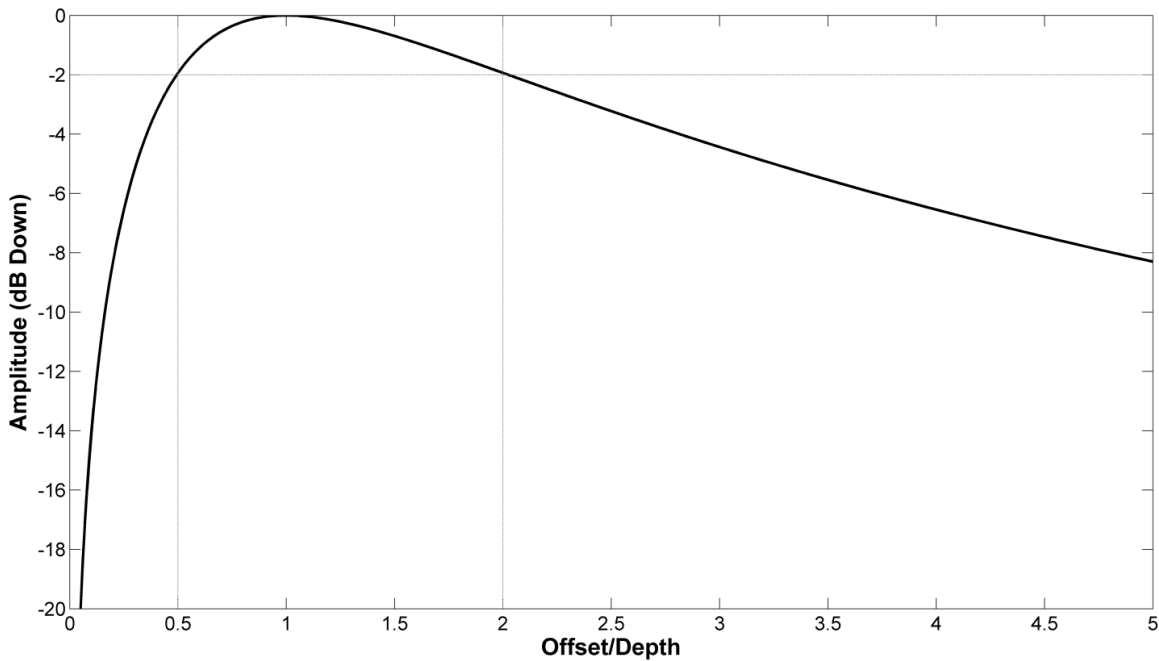


FIG. 20. Modeled relative amplitude change of the horizontal components of a borehole geophone, as a function of the source-well offset/receiver depth ratio. Horizontal line is drawn in at -2 dB, which intersects the curve at offset/depth ratios of approximately 0.5 and 2.

Estimates of signal to noise ratio were found for each trace of the rotated horizontal (H_{\max}) components, and the values were plotted against source-well offset (FIG. 21). The estimate was made by calculating the RMS amplitude of the first break window of a trace, which was 100 ms long, and dividing it by the RMS amplitude of the first 100 ms of that trace, which was considered noise. The results here provide a good match to what was modeled; however, the peak amplitude occurs at a source-well offset that is smaller than the geophone depth. This is likely due to the effects of raybending, which will cause the incoming ray at the receiver to be closer to horizontal than expected for a homogeneous medium (FIG. 22).

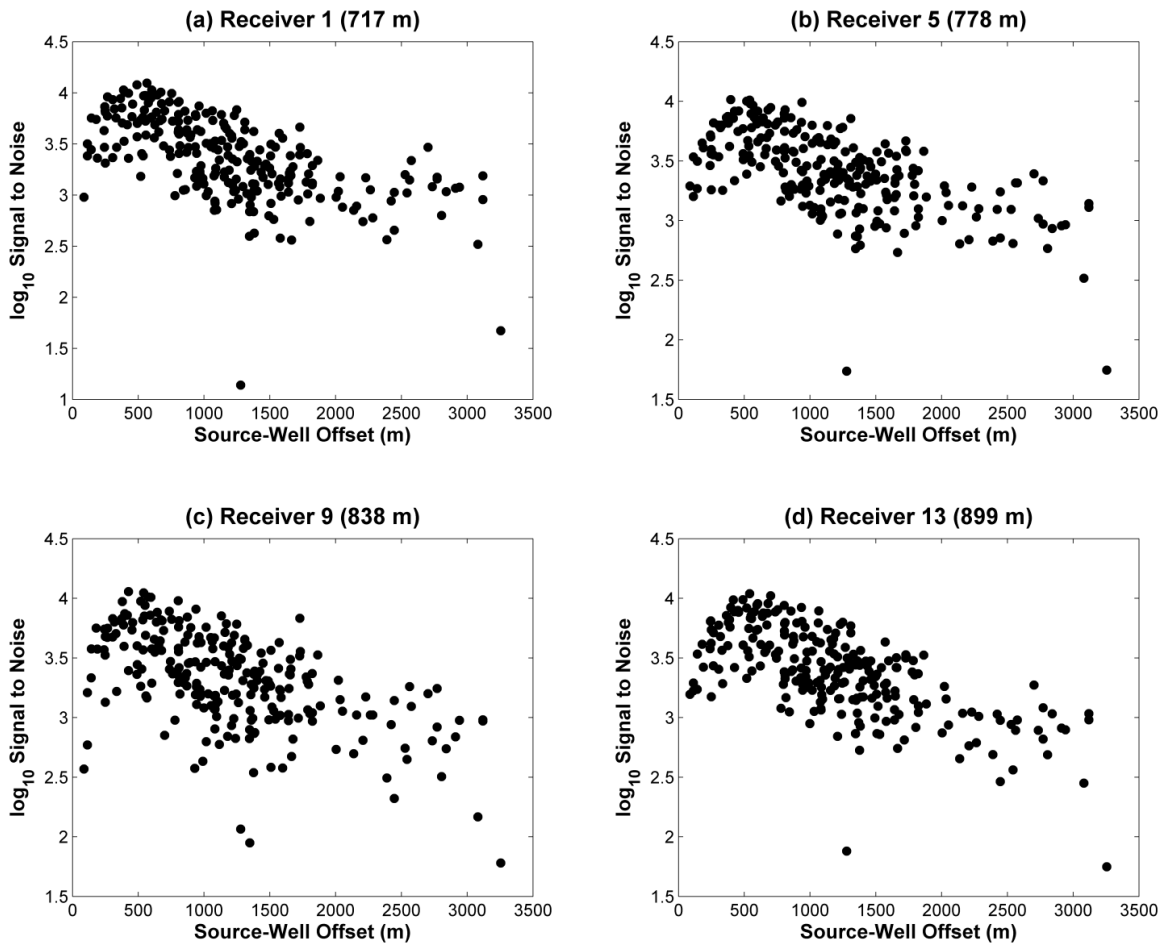


FIG. 21. Estimated signal to noise of first break window, versus offset, for the H_{\max} component of a subset of receivers in the 3D dataset. Data were rotated using angle estimates from the analytic method.

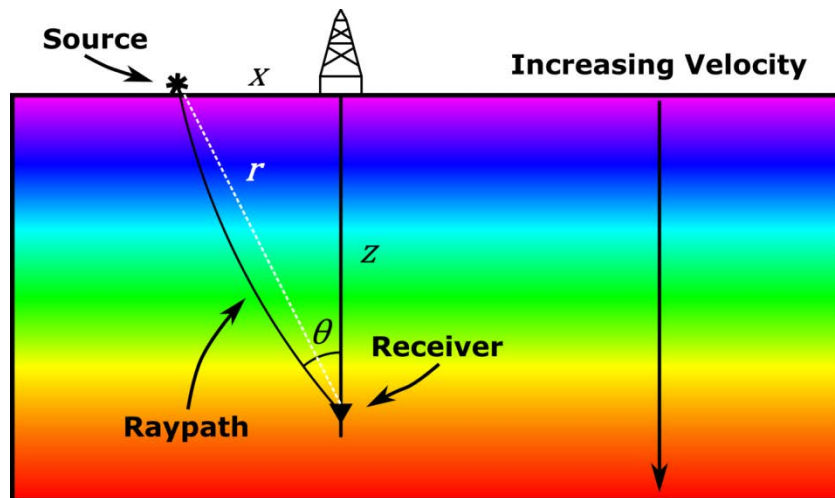


FIG. 22. Illustration of raybending that would occur due to a linear velocity gradient where velocity increases downwards.

DISCUSSION

The geophone orientation azimuths calculated in this study, for both the 3D and 2D walkaway surveys, resulted in robust outcomes. The 2D walkaway data showed similar scatter in orientation azimuth when for all 3 walkaway shot lines, but the scatter in the 3D walkaway data changed significantly when the data were split into separate bins, although mean angles were very similar. Additionally, the removal of shots from source-well offsets less than about 1/2 of the geophone depth had a large effect on the 2D walkaway orientation statistics, while having less effect on the 3D dataset. This is probably due to the low proportion of near offset source locations in the 3D walkaway survey.

The results found using the azimuthally binned (3D walkaway) and line by line (2D walkaway) analysis do not show any clear indication that, in this area, there is significant source-well azimuthal dependence on computed borehole geophone orientations. Mean angles were very consistent regardless of the bin or line chosen; differences are generally no greater than the standard deviations involved, nor are there any consistent trends for a particular bin or line. Direct examination of the orientation angle versus source-well azimuth in the 3D walkaway shows only a subtle trend. The consistency of the orientation azimuths can be interpreted to mean that the local geology is likely azimuthally consistent, which is expected from flat, isotropic layers.

The offset binning of the 3D dataset showed a strong dependence of geophone orientation scatter to source-well offset. For all 15 working receivers, scatter was reduced in the 600-1650 m offset range, reaching a minimum in the 1300-1650 m bin. Scatter in the bins containing offsets less than 600 m and greater than 1650 m was significantly higher, which is due to a combination of effects. First, the signal to noise of the first arrival on the horizontal components is reduced in these two offset ranges; the near offsets will have a near-vertical angle of incidence, and the far offsets will be more affected by geometric spreading. Second, analysis of orientation angle is more sensitive to source positioning errors at near offsets. Thus, for the 3D dataset, the optimal offset range to perform orientation analysis was between 1 and 2 times the receiver depth. Modeling of the amplitude change in a homogeneous, isotropic medium with high quality factor confirms this, predicting an optimal source-well offset equal to the receiver depth.

Finally, comparison of the analytic and hodogram methods revealed that the two are very similar, though the analytic method gave slightly less scatter in computed azimuths. The mean of the two methods rarely differed by greater than 1° and on average differed by less than 0.5° . The similarity of results through both of these methods gives confidence that each of them can estimate reliable information about geophone orientation.

CONCLUSIONS

- Geophone orientations for the 2D dataset were determined using the DiSiena et al. (1984) analytic method. The standard deviation was 0.67° for all lines, 0.45° for the east line, 0.41° for the southeast line and 0.55° for the south line.

- Geophone orientation angles for the 2D dataset were also found using a linear regression, or hodogram, method. The standard deviation was 0.9° for all lines, and 0.77° for the east line, 0.42° for the southeast line and 0.62° for the south line.
- Absolute difference in mean angles between the two methods averaged 0.12° for all lines, and 0.14° , 0.12° and 0.17° for separate lines.
- Geophone orientation angles for the 3D dataset were found using the analytic method. The standard deviation was 1.74° using all azimuths, and became 1.23° , 0.35° , 0.90° and 1.85° when the data were binned into centers of 0° - 180° , 45° - 225° , 90° - 270° and 135° - 315° respectively.
- Signal to noise in the rotated horizontal component reached a maximum where the source-well offset was approximately equal to geophone depth.
- Scatter in orientation angle for the 3D dataset reduced noticeably as source locations became more than 600 m from the well. The scatter minimized in the offsets between 1300 and 1650 m.
- The optimal offset range for geophone orientation calibration was found to be in the range of 1-2 times the receiver depth.
- Removal of data points nearer than 1/2 of the receiver depth reduced the scatter of orientation angles in the unbinned 3D walkaway, from 2.41° to 1.74° . It significantly improved the scatter in the 2D walkaway surveys, decreasing the standard deviation from 5.22° to 0.67° overall.
- For both the 3D and the 2D walkaways, the geophone orientations were not found to have any consistent dependence on source-well azimuth. This is expected for flat, isotropic geology near the well.
- The analytic and linear regression methods of calculating geophone orientations produced comparable results overall; however, the analytic method was found to consistently give slightly less scatter.

ACKNOWLEDGEMENTS

We would like to thank EnCana and Schlumberger for providing the data used in this study, and GEDCO for the use of their Vista software. We would also like to thank CREWES Sponsors and Carbon Management Canada for their continued support of this research.

REFERENCES

- DiSiena, J. P., Gaiser, J. E. and Corrigan, D., 1984, Three-component vertical seismic profiles; orientation of horizontal components for shear wave analysis, in Toksoz, M. N. and Stewart, R. R., eds., *Vertical seismic profiling, Part B Advanced concepts*, 189-204.
- Eisner, L., Duncan, P. M., Heigl, W. M. and Keller, W. R., 2009, Uncertainties in passive seismic monitoring: *The Leading Edge*, **28**, 648-655.

- Gagliardi, P. and Lawton, D. C., 3D borehole geophone orientation study, central Alberta: CREWES Research Report **23**, 28.1-28.27.
- Le Calvez, J. H., Bennett, L., Tanner, K. V., Grant, W. D., Nutt, L., Jochen, V., Underhill, W. and Drew, J., 2005, Monitoring microseismic fracture development to optimize stimulation and production in aging fields: *The Leading Edge*, **24**, 72-75.
- Li, X. and Yuan, J., 1999, Geophone orientation and coupling in three-component sea-floor data: a case study: *Geophys.Prospect.*, **47**, 995-1013.
- Müller, K. W., Soroka, W. L., Paulsson, B. N. P., Marmash, S., Al Baloushi, M. and Al Jeelani, O., 2010, 3D VSP technology now a standard high-resolution reservoir-imaging technique: *The Leading Edge*, **29**, 686-697.